Finite Element Stress Analysis and Vibration Analysis for a Geothermal Separator

Ohgeon Kwon[1] and Annette Karstensen[2]

[1]Quest Integrity (NZL) Limited, PO Box 38096, Lower Hutt 5045, New Zealand

[2]Quest Integrity AUS Pty Limited, 1/482 Scottsdale Drive, Varsity Lakes 4227, QLD, Australia

o.kwon@questintegrity.com, a.karsetensen@questintegrity.com

Keywords: geothermal separator, fatigue, corrosion, cracking, finite element stress analysis, vibration analysis, repair options

ABSTRACT

A geothermal separator that experienced fatigue and corrosion fatigue cracking on the internal stand pipe attachments was subjected to an advanced engineering critical assessment including Finite Element stress analysis and vibration analysis to define the root cause of the cracking. The developed Finite Element model was used to analyse proposed mechanical arrangements to reduce the risk of cracking in future. Repair options were identified and a successful repair method was achieved.

1. INTRODUCTION

The high pressure (HP) steam separator failed at the internal stand pipe attachments following three months of service. According to the failure investigation, the crack initiation and subsequent propagation was due to cyclic fatigue. The fatigue cycles were primarily due to resonance of the centre pipe and possibly random flow vibrations.

Possible repair options were examined using Finite Element (FE) analyses including linear static stress analysis, computational fluid dynamic (CFD) analysis, natural frequency and mode analysis, transient dynamic analysis and fatigue assessment. The most effective repair option was designed for avoidance of reoccurrence of cracking and failure of the pipe attachment by reducing peak stress level and fatigue stress amplitude from revised design.

This paper describes relevant FE analyses as a process of repair option development and how a successful repair method was identified.

2. FE ANALYSIS

2.1 Linear elastic static analysis

The linear elastic static FE analysis was carried out to determine the stresses of the HP Separator for the original design, with 4 struts of the HP Separator and 8 struts modified model using the steady state operating pressure data. The objectives of these analyses were to determine the stress distribution at the strut-shell and strut-pipe joints as a result of the uniform operating pressure conditions.

The main dimensions of the HP Separator are as follows:

- Shell Thickness and diameter: 28mm, 25mm, 38mm & ID: 3352mm
- Pipe Thickness and diameter: 16mm, 10mm & ID: 1199.2mm
- Strut Thickness and diameter: 15mm & ID: 59mm

2.1.1 Finite element model

FE analyses of the HP Separator were undertaken to obtain the stresses generated at the joint between the pipe, the shell and the struts due to the internal pressure. A uniform internal pressure of 11.57 bar (1.157 MPa) was applied to the model. A three dimensional FE model of the 4 struts and 8 struts HP Separator was developed using ABAQUS FE software (Abaqus/CAE V6.9).

2.1.2 Stress analysis and results

A linear elastic FE analysis was carried out on the HP Separator model subject to the internal uniform pressure applied between the external surface of the pipe and the struts. The hoop stress contours are illustrated in Figure 1. A close up of the hoop stress distributions around the top strut joint in the pipe side as well as the shell side are shown in Figure 2 and Figure 4. A path was defined to provide stress profiles of the external and internal surfaces of the pipe and shell particularly the area adjacent to the struts, as shown in Figure 3 and Figure 5 for comparison.

The stress analysis revealed that:

- Maximum stresses (146MPa) occurred at the joint between the strut and the central pipe. The stress distribution around the joint appeared to be a "horse shoe" pattern. This is consistent with the cracking seen in the failed strut joints
- Maximum stress between the strut and the shell wall was determined as 116MPa
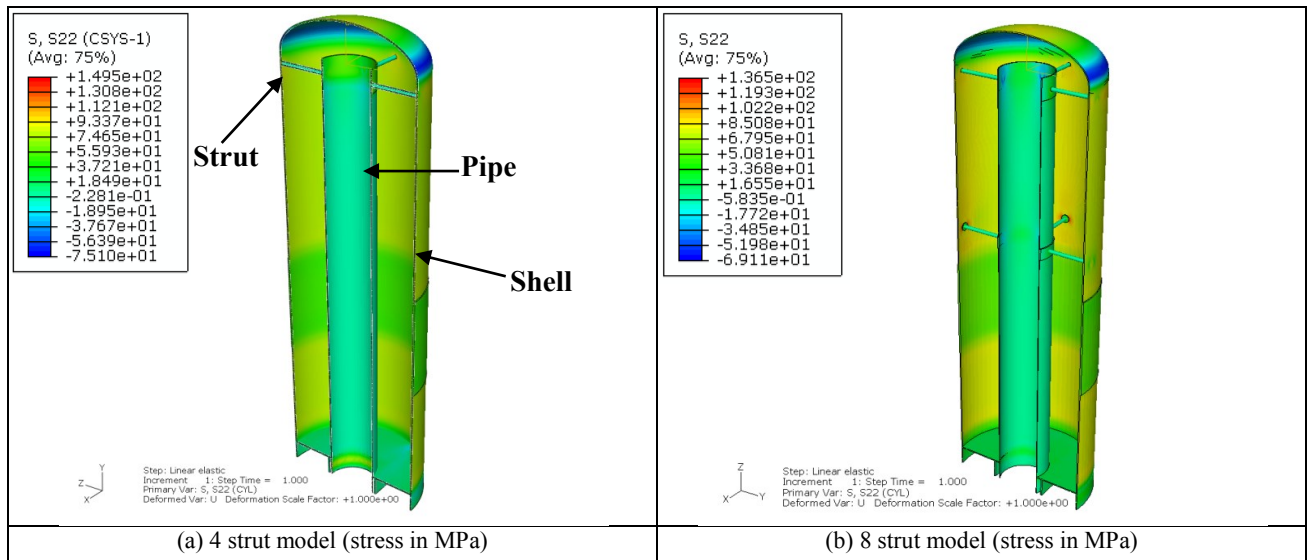- The stresses in the pipe at the top struts slightly decreased in the 8 struts model.

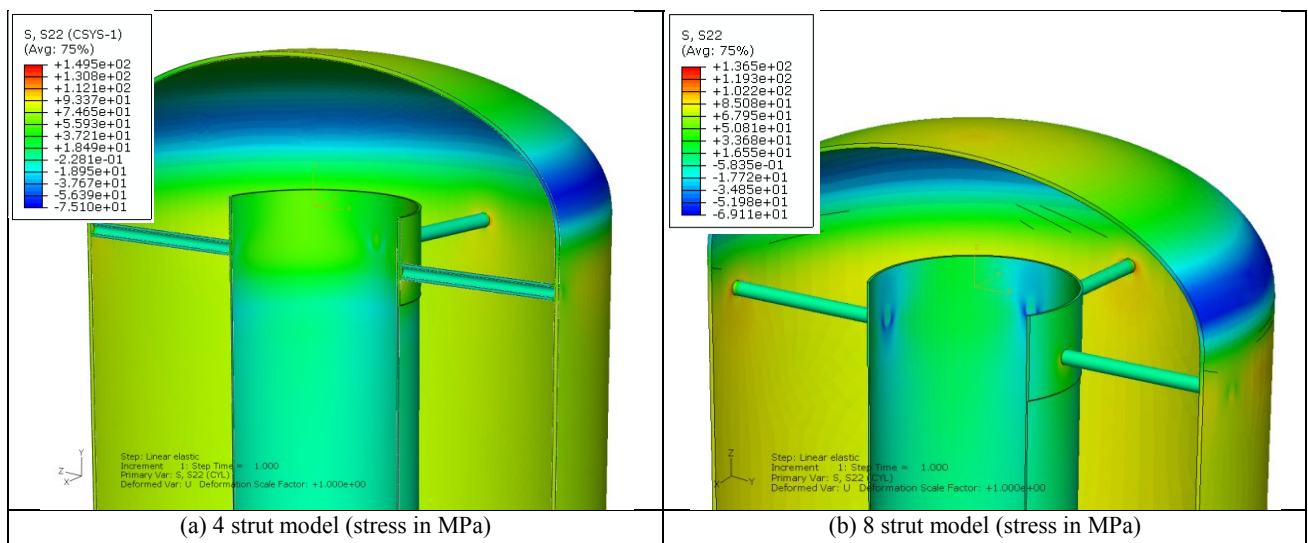| (a) 4 strut model (stress in MPa) | (b) 8 strut model (stress in MPa) |

Figure 1: Hoop stress distribution

| (a) 4 strut model (stress in MPa) | (b) 8 strut model (stress in MPa) |

Figure 2: Stress distribution around Hoop the Top struts.
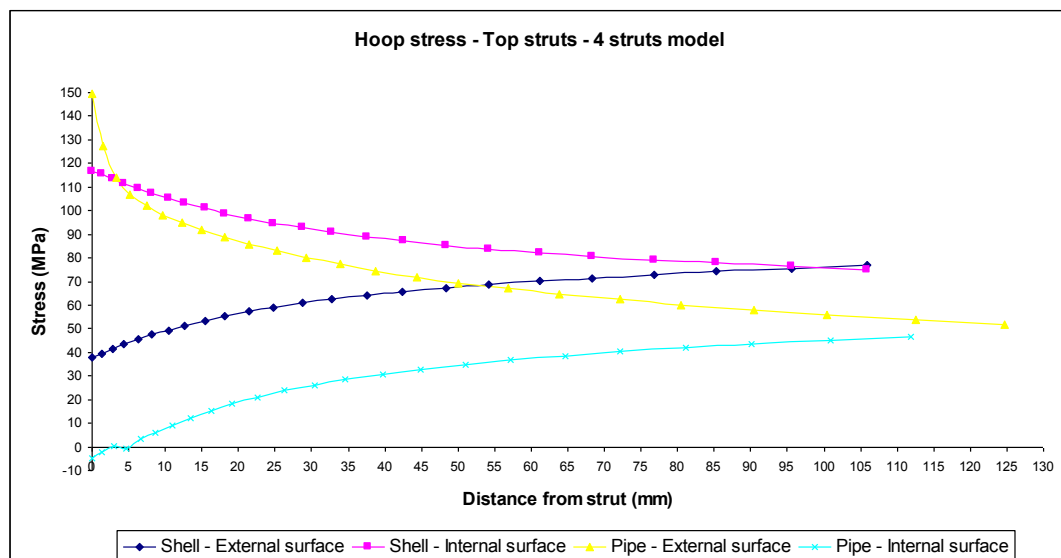
Figure 3: Hoop stress profile – Top struts (4 struts model).

2

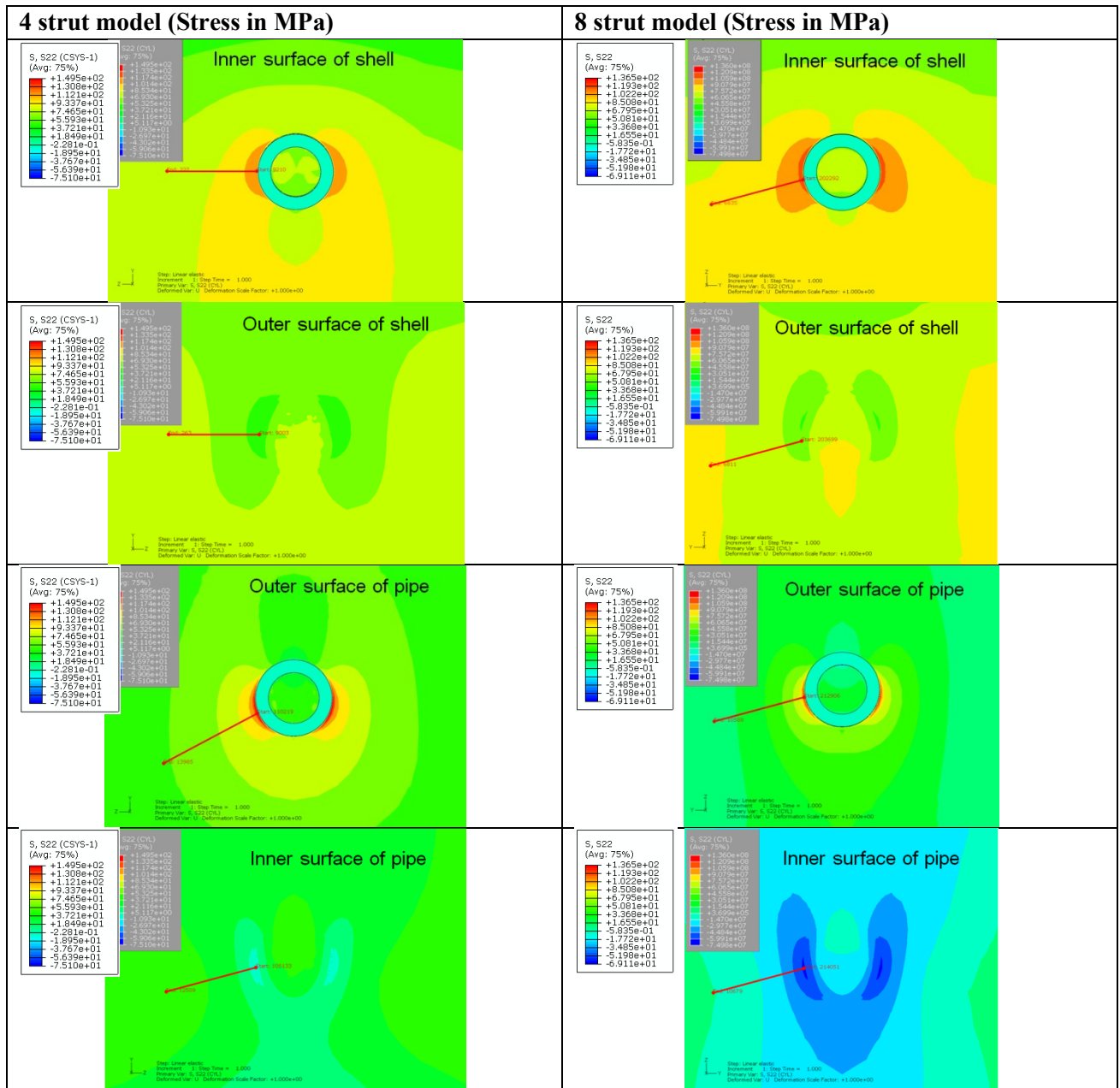| 4 strut model (Stress in MPa)	8 strut model (Stress in MPa)
Inner surface of shell	Inner surface of shell
Outer surface of shell	Outer surface of shell
Outer surface of pipe	Outer surface of pipe
Inner surface of pipe	Inner surface of pipe

Figure 4: Hoop stress distribution around the strut joint with the shell and the pipe – Top struts.
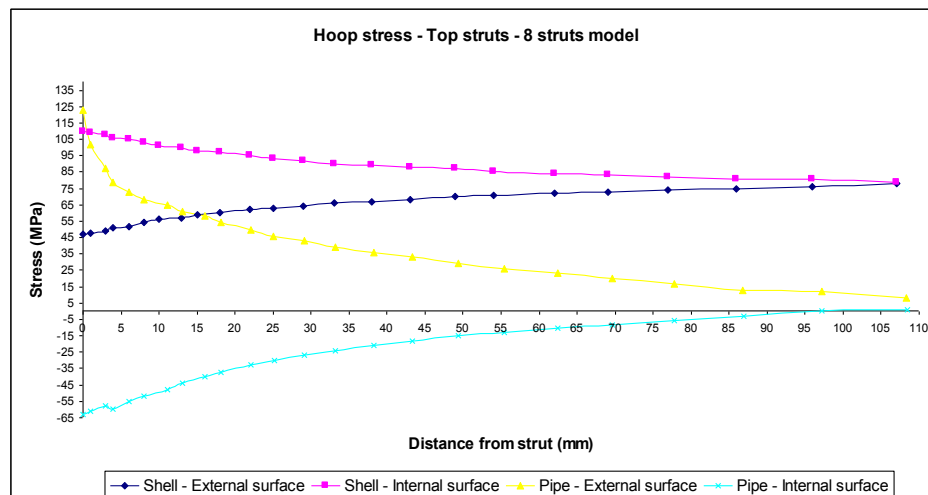

Figure 5: Hoop stress profile – Top struts (8 struts model).

3

2.2 Natural frequency and modal analysis

The natural frequencies for the original design with 4 struts of the HP Separator was analysed and compared with that of the modified design with 8 struts. When the resonance frequency is approximately equal to the natural frequency of the system, resonant phenomena occur and small periodic driving forces can produce large amplitude vibrations.

The model was generated using the pre-processor CEA and the analysis was conducted employing the general purpose FE package ABAQUS. The natural frequency and mode shapes were obtained using the Lanczos eigensolver as available in ABAQUS for modal analysis. The natural frequency associated with each eigenmode of the 4 struts model and 8 struts model up to three eigenmodes are illustrated in Figure 6.

The lowest natural frequency was 20.9 Hz for 4 struts model and 21.9 Hz for 8 struts model. The corresponding mode shape was distortion of the top of the pipe section in triangular shape along with bent struts for both models. There was no significant difference in the natural frequency and mode shape of the first eigenmode between two models.
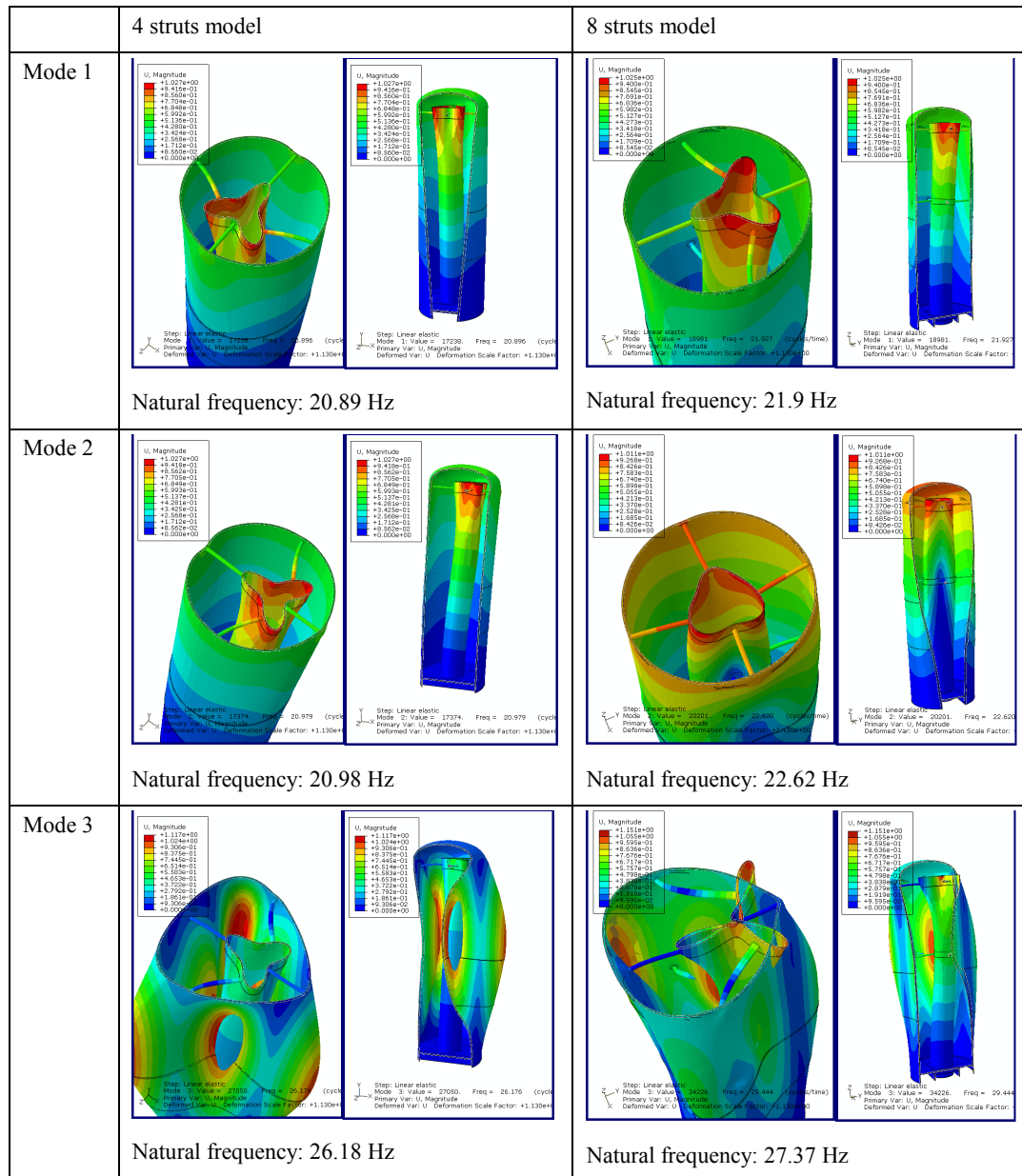
	4 struts model	8 struts model
Mode 1	Natural frequency: 20.89 Hz	Natural frequency: 21.9 Hz
Mode 2	Natural frequency: 20.98 Hz	Natural frequency: 22.62 Hz
Mode 3	Natural frequency: 26.18 Hz	Natural frequency: 27.37 Hz

Figure 6: Comparison of natural frequency and mode shape of the first three eigenmodes.

2.3 FE analysis of HP Separator using CFD pressure mapping data

The steady state computational fluid dynamics (CFD) analysis for the HP Separator revealed a significant differential pressure at the top of the inner pipe as a result of unstable steam flow. The differential pressure observed at the top of the inner pipe results in additional load and vibration, and consequently the cyclic stresses generated by this load is likely impose fatigue damage on the joint between the pipe and struts. The static FE analysis imposing the steady state condition from CFD analysis was carried out to determine the difference in fatigue stress range between the original design with 4 struts and 8 struts modified model.

The provided pressure distribution data from the steady state CFD analysis are shown in Figure 7.The pressure mapping data was transferred from the steady state CFD model and applied to the FE model to carry out the static stress analysis. Figure 8 shows the applied loading condition on FE model transferred from CFD analysis. The same geometry and material properties of the HP Separator used in the static stress analysis from uniform internal pressure was used.
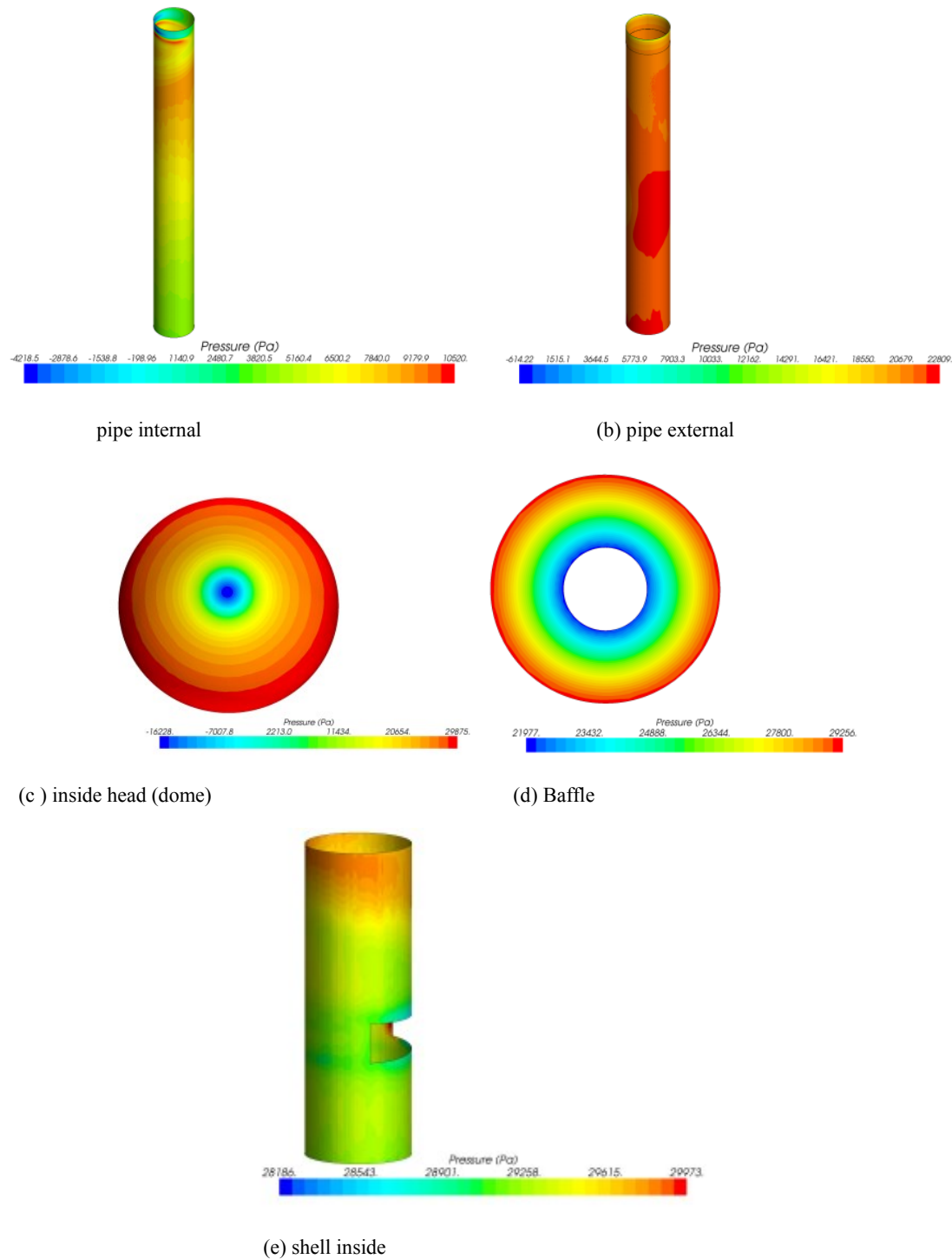

pipe internal

(b) pipe external

(c) inside head (dome)

(d) Baffle

(e) shell inside

Figure 7: Pressure distribution from CFD analysis. (Pressure loading in Pa)

FE analyses of the HP Separator were undertaken to obtain the stresses generated at the joint between the pipe and struts due to the pressure differential as a result of unstable steam flow into the pipe.

A linear elastic FE analysis was carried out on the HP Separator models subject to the pressure differential from CFD steady state analysis. The elastic stresses around the joint between the external surface of the pipe and the struts are shown in Figure 9. Two paths were defined to provide stress profiles adjacent to the top struts, as shown in Figure 9. Path 1 considers the stress of the pipe external surface left hand side of the strut and Path 2 considers the stress at the right hand side of the strut. The hoop stress profiles along the paths defined are shown for 4 struts model and 8 struts model in Figure 10 and Figure 11.
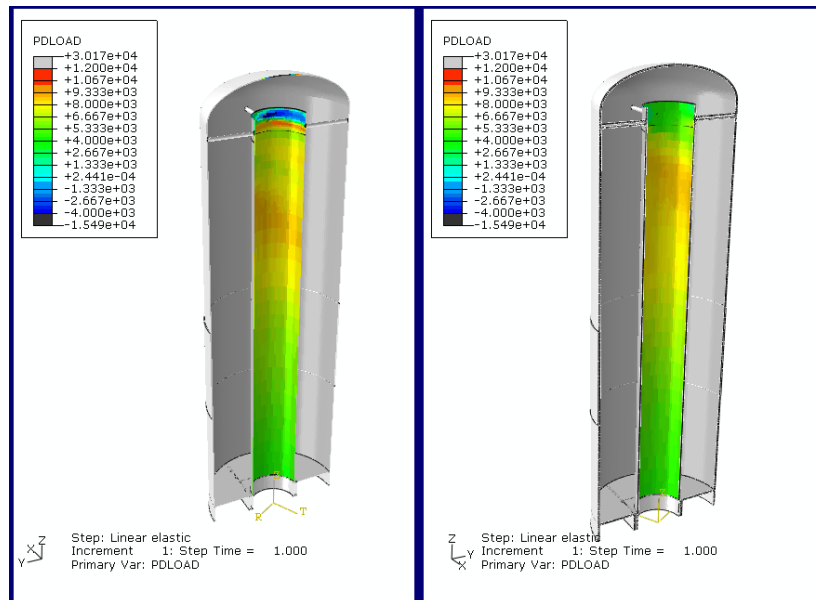
Figure 8: Applied loading condition to the inner pipe for FE static analysis from CFD pressure mapping (Pressure loading in Pa).
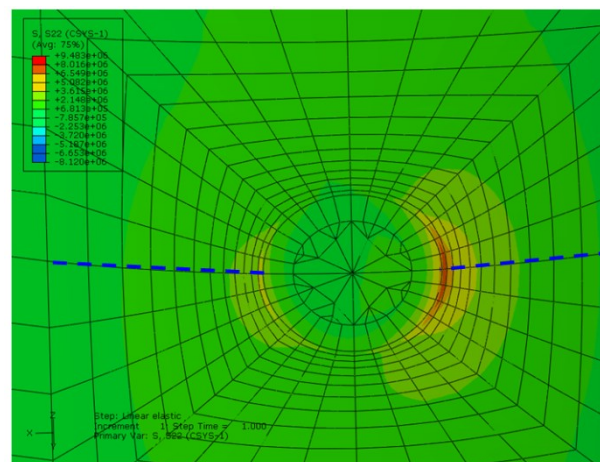

Figure 9: Stress (Hoop stress in Pa) distribution in the external surface of the pipe around one of the struts in the 4 struts model (blue dotted lines indicate the path for stress evaluation).
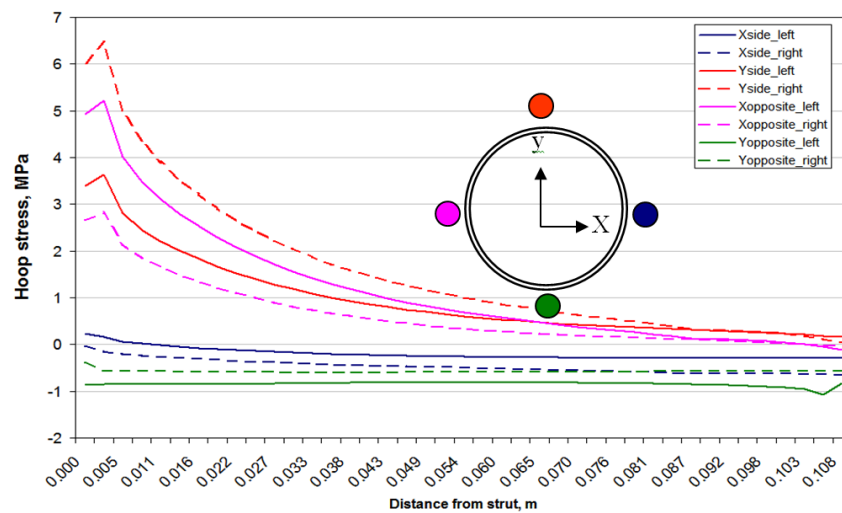

Figure 10: Stress distribution of the external surface of the pipe around the struts (4 struts model).
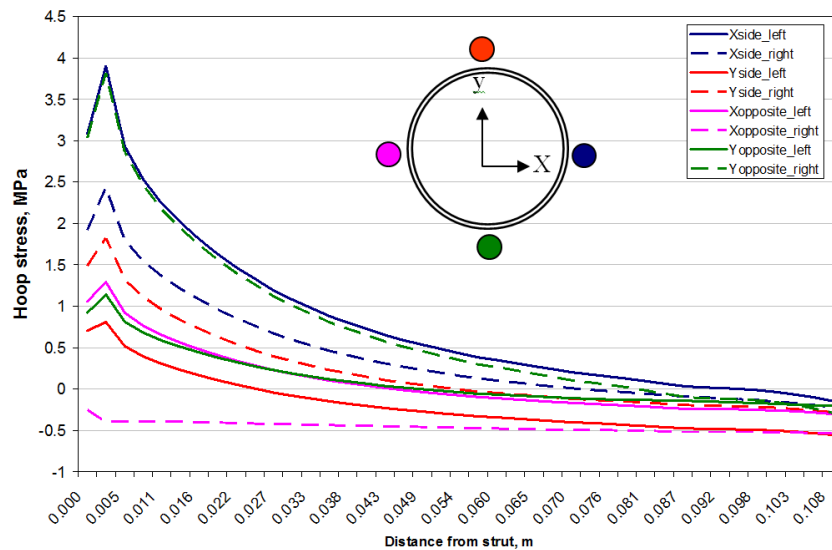
Figure 11: Stress distribution of the external surface of the pipe around the struts (8 struts model).

The stress analysis revealed that:

- Maximum stress amplitude from pressure fluctuation was 6.5MPa for 4 strut case and 3.9MPa for 8 strut case. The stress level at the joint between the strut and the pipe varied depending on the location of the strut.
- Non-symmetric stress distribution around strut was obvious, mainly due to bending moment imposed on the strut. The stress value at one path was approximately 50% less than that at the other path. The deformation of the top of the pipe with respect to the struts was consistent with the stress distribution seen, see Figure 12.
- The stresses on the outside of the pipe to strut welded joints in the 4 struts model were higher than on the 8 struts model.
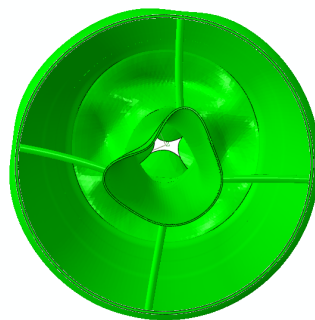

Figure 12: Deformation of the pipe and struts showing maximum bending moment at the joint between the pipe and the struts.

2.4 Repair option study

Six possible repair options were considered as follows:

0: current configuration (with midheight struts)
1: collar at top of pipe thickened to 28 mm
2: struts moved to 1500 mm below top of pipe (16 mm collar extends from top to 1700 mm below top)
3: top strut rotated 15º (about vertical rotation axis)
4: struts pinned at either end
5: top struts rotated 45º (struts run downhill going from shell to pipe, with 16 x 500 mm tall collar)
6: all struts rotated 15º (about vertical rotation axis), donut at top of pipe

All repair options were evaluated using hoop stress in the center pipe adjacent to the strut-pipe weld and internal pressure (11.7 bar) on the vessel interior. Stresses were measured along the meridional path starting at the center of the strut at the pipe/wall. Hoop stress distributions at the shell and pipe were compared for the repair options analysed.

Repair options were ranked according to ratio of hoop stresses in the pipe, comparing repair option to current configuration (see Table 1). Stresses are at the pipe outer surface at (an arbitrary) 10 cm away from center of strut. The 6th option with the donut shape

at the top of the pipe (see Figure 13) was found to be the most effective option in terms of reduction of stress at the pipe. However, there was no significant reduction in stress at the shell wall.

Table 1: Ranking of repair options in terms of ratio of hoop stresses in pipe

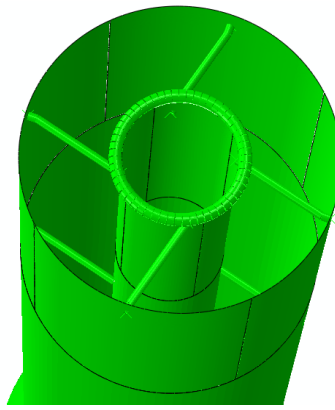| Repair option	Stress in pipe		Stress in wall, MPa
	Stress, MPa	Compared to current configuration	
6: all struts rotated 15° + donut	8.4	24%	99.6
2: struts moved to 1500 mm below	22.7	66%	101.5
3: top struts rotated 15°	26.8	78%	94.1
1: 28 mm collar on pipe	28.1	82%	103.8
4: struts pinned	34.2	100%	96.2
5: top struts angled 45° down	54.7	159%	103.3

Figure 13: Repair option with donut shape of top of the pipe.

3. FATIGUE ASSESSMENT OF REPAIR KITS

Fatigue assessment was carried out based on the stresses developed for two final suggested designs, see Figure 14:

1.   The repair kit designed by Original Equipment Manufacturer (OEM).

2.   The repair kit suggested (the donut design).
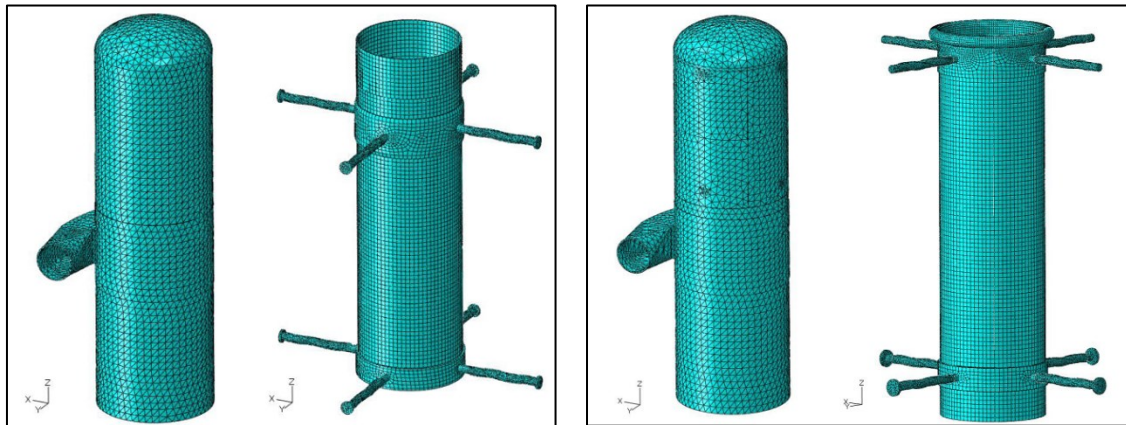
(a)   OEM design   (b) Suggested repair kit (donut shape pipe top)

Figure 14: Repair solution suggested by OEM and the repair solutions including a donut.

A literature review was carried out on the fatigue performance of steels in geothermal steam (Chung and Karstensen, 2009). Very limited data has been published for carbon steel welds, however the data that was available showed consistent results with regards

to the fatigue performance. The evidence was that for the same stress there is a 10 times reduction in the number of cycles to failure in geothermal steam compared to air. Based on this evidence, Figure 15 shows the recommended fatigue curve to be used for the strut to steam pipe welds and strut to shell welds in the HP Separator.

In accordance with BS7608 (British Standard Institute, BS 7608:1993), there is a certain stress range below which an indefinitely large number of cycles can be sustained. This stress range depends on the environment, for example in seawater with adequate corrosion protection and in air, the stress range corresponds to 10^7 cycles to failure by the design fatigue endurance curve (S-N curve). In accordance with the literature review "run outs", no failure was experienced in the test carried out in geothermal steam before 10^7 cycles and therefore it has been assumed that the threshold for no fatigue initiation and propagation will be at 10^7 cycles for the current environment. This corresponds to a maximum allowable stress range on the strut welds of 18MPa.
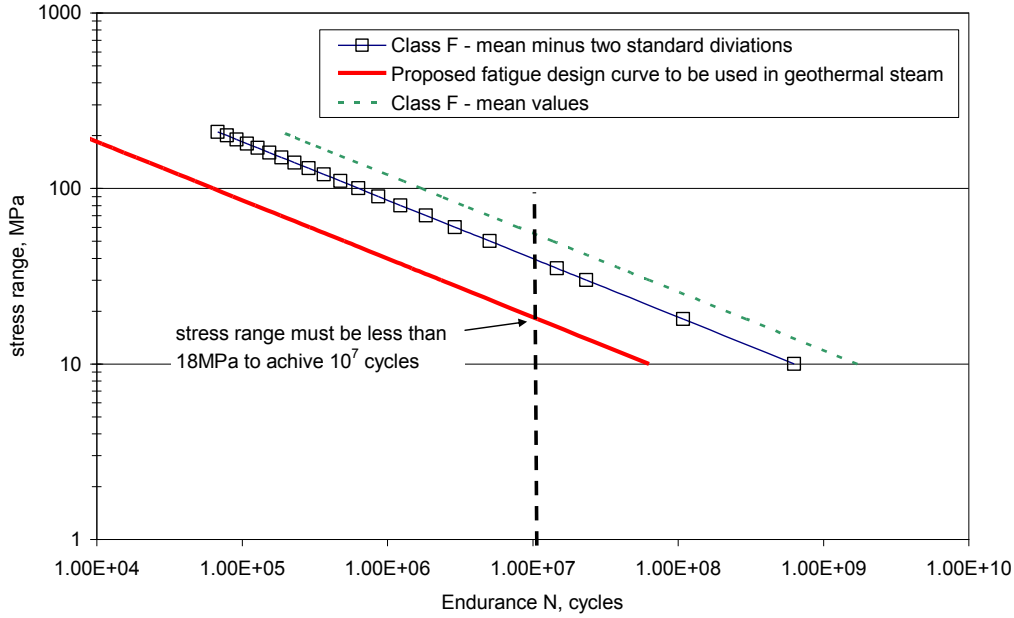

Figure 15: The S-N curve recommended for the pipe to strut joint in the HP Separator. The dotted line is the mean of values for a Class F joint (BS7608), the solid line with squares is the mean minus two standard deviations. The red solid line represents a 10 times reduction in number of cycles to reach the endurance limit compared to the mean minus two standard deviations.

The transient dynamic analyses of the global models were conducted using a time step size of 0.001s over a time period of 1.6s to determine the structural modes that have been excited by the fluid loading and show that the response in this direction is dominated by the structural modes. The presence of the stays had the effect of smearing the frequency content of the fluid excitation. Most importantly the amplitude of the reaction force oscillations is significantly smaller in the donut case which indicates that the level of fluid excitation is much lower in this case.

The maximum and minimum principal stresses were presented as a function of time in a time span of 1.6sec, see for example Figure 16. The stress ranges ($\Delta\sigma$) were calculated as the difference between σ_p and σ_d. It can be seen that most of the stress ranges are below the threshold level of 18MPa. This implies that most of the cyclic stresses do not contribute to the fatigue initiation, as only one stress range within the 1.6 second analysis exceeds 18MPa.

The fatigue damage has been calculated as follows:

$$D = \sum \frac{n_1}{N_1} + .. + \frac{n_i}{N_i}$$

Where n_i is the number of cycles at the i stress range and N_i is the number of cycles to failure at the i stress range. The values of N are determined from the red line in Figure 2. Failure is reached when the damage factor accumulates to a value of 1.

Therefore the total number of cycles for the damage factor to reach a value of 1 has been calculated for each analysed case.

A comparison between the two designs has been made of the damped models. This has been done by assuming that all cycles are contributing to failure (i.e. no threshold) and calculating the accumulated damage in the highest stressed location. The results are summarised in Table 2. It can be seen that the stress ranges in the donut repair model are 14 times less severe than those generated in the OEM model.
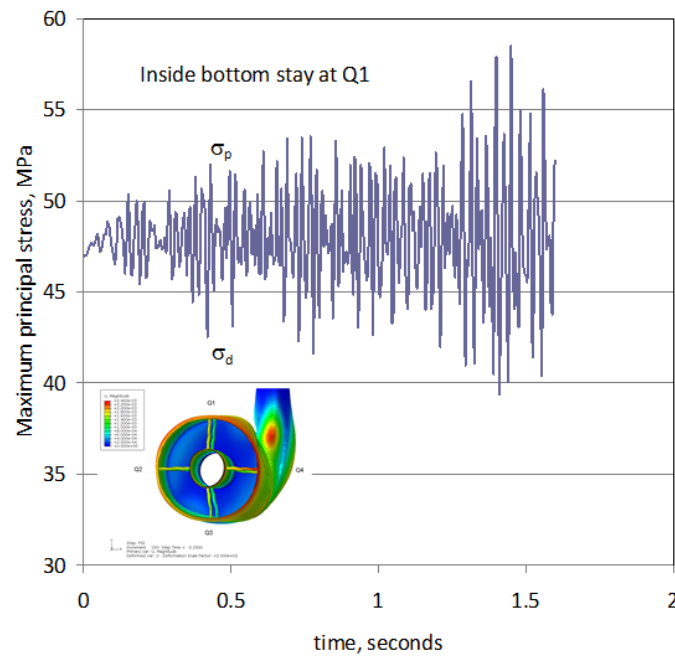
Figure 16: Showing an example of the maximum principal stresses as a function of time.

Table 2: Fatigue performance when a threshold is not considered (results only for comparison between the two models).

Model	Accumulated damage per cycle not considering a threshold	Number of cycles to failure not considering a threshold
OEM design	2.18×10^{-7}	2.53×10^{8}
Donut repair kit	1.50×10^{-8}	3.13×10^{9}

4. CONCLUSIONS

From the FE analyses and fatigue assessment the following can be concluded:

- FE stress analysis confirmed that the relatively high stress distribution with "horse shoe" pattern at the connection to the outer shell was consistent with the cracking seen in the HP separator. This was due to the steam tube and stays preventing outward movement of the shell due to internal pressure at these points, which creates a bending action at the outside of the reinforcement pads.
- Increased number of struts reduced stress in the strut joint, however, there was no significant effect in the natural frequency and mode shape.
- Pressure differential observed at the top of the inner pipe of the HP Separator as a result of unstable steam flow into the inner pipe was likely the main source of fatigue cycles on the joint between the pipe and struts. The stresses on the outside of the pipe to strut welded joints in the 4 struts model were higher than the 8 struts model.
- The repair kit option with the donut shape at the top of the pipe was found to be the most effective option. A comparison in fatigue performance between the OEM design and the donut repair option showed that the damage accumulated was 14 times less in the donut design than in the OEM design.
- When considering structural damping, the fatigue stress ranges as a result of the pressure differential are below the threshold level for fatigue initiation, which was proved to be a successful repair method.
- Following repairs and slight design modifications, the vessel was returned to service.

REFERENCES

Abaqus/CAE V6.9. Dassault Systèmes Simulia Corp., Providence, RI. USA. 2009.

Olivia Chung and Annette Karstensen: Literature Review of the Fatigue Performance in a Geothermal steam environment, Quest Reliability report, May 2009.

British Standard Institute, BS 7608:1993, "Code of practice for fatigue design and assessment of steel structures".